J. Fluid Mech. (1989), *vol.* 199, *pp.* 441–469
Printed in Great Britain

Frequency selection and asymptotic states in laminar wakes

By GEORGE EM KARNIADAKIS† AND GEORGE S. TRIANTAFYLLOU‡

† Department of Mechanical and Aerospace Engineering, Princeton University, D209-A, Princeton, NJ 08544, USA

‡ Department of Ocean Engineering, MIT Room 5–426A, Cambridge, MA 02139, USA

(Received 16 October 1987 and in revised form 3 May 1988)

A better understanding of the transition process in open flows can be obtained through identification of the possible asymptotic response states in the flow. In the present work, the asymptotic states in laminar wakes behind circular cylinders at low supercritical Reynolds numbers are investigated. Direct numerical simulation of the flow is performed, using spectral-element techniques. Naturally produced wakes, and periodically forced wakes are considered separately.

It is shown that, in the absence of external forcing, a periodic state is obtained, the frequency of which is selected by the absolute instability of the time-average flow. The non-dimensional frequency of the vortex street (Strouhal number) is a continuous function of the Reynolds number. In periodically forced wakes, however, non-periodic states are also possible, resulting from the bifurcation of the natural periodic state. The response of forced wakes can be characterized as: (i) lock-in, if the dominant frequency in the wake equals the excitation frequency, or (ii) non-lock-in, when the dominant frequency in the wake equals the Strouhal frequency. Both types of response can be periodic or quasi-periodic, depending on the combination of the amplitude and frequency of the forcing. At the boundary separating the two types of response transitional states develop, which are found to exhibit a low-order chaotic behaviour. Finally, all states resulting from the bifurcation of the natural state can be represented in a two-parameter space inside 'resonant horn' type of regions.

1. Introduction

There has recently been a renewed interest in the formation of vortex streets in the wake of bluff objects and the physical mechanisms dictating their states. The flow past a circular cylinder, in particular, has served for nearly a century now as a model for fundamental studies of external flows. Morkovin (1964) has aptly characterized the flow past a cylinder as 'a kaleidoscope of challenging fluid phenomena', referring to the variety of fluid structures and different flow regimes that are observed in this flow. Since then, a vast volume of literature has been added to the subject, mostly concerning the formation of the wake and the frequency selection process.

To the list of long-conflicting experimental results of Tritton (1959, 1971), Gaster (1969), and Berger & Wille (1972) about the frequency selection in the wake of circular cylinders, the findings of Friehe (1980), Sreenivasan (1985) and Van Atta & Gharib (1987) have been added more recently. An attempt was made in the more recent studies to explain discontinuities in the Strouhal number (St) versus Reynolds

number (Re) relationship, first reported by Tritton (1959), in the light of contemporary theories relating the development of turbulence in fluids to the presence of strange attractors (Ruelle & Takens 1971). In his controversial paper, Sreenivasan (1985) attributed the discontinuities in the Strouhal-versus-Reynolds number relationship to the presence of chaotic patterns in the wake of the cylinder. Sreenivasan (1985) claimed that such patterns develop even for Reynolds numbers below 100, for which the wake is still laminar (Bloor 1964). He described the formation of chaotic patterns as following the theoretical scenario suggested by Newhouse, Ruelle & Takens (1978) (usually referred to as the 'RTN' scenario). The results of Sreenivasan (1985), however, were recently disputed by Van Atta & Gharib (1987). They demonstrated convincingly that the chaotic state of the flow observed by Sreenivasan (1985), and the discontinuities observed by Tritton (1959), were in fact due to aeroelasting coupling between the vortex wake and the cylinder vibration modes. According to Van Atta & Gharib (1987), chaotic states in a laminar wake do not result from purely fluid-mechanical origins; they can only be created from external forcing, or aeroelastic coupling, following the scenario of 'pattern competition' proposed by Ciliberto & Gollub (1984) in the context of a different physical problem.

The fact remains that quasi-periodic and chaotic states, whether due to purely fluid-mechanial phenomena or aeroelastic coupling, are possible in low-Reynolds-number flows. The origin and development of such patterns are worth investigating, because they can offer significant insight into the transition process in laminar flows. From the application point of view, identification of states in 'open' flows is important for flow-control problems. The goal in flow-control problems may be cancellation of unsteady patterns, like in vibration-suppression applications, or reinforcement of unsteady patterns, like in transport enhancement applications. For both types of problems, choosing the appropriate control device can be guided from investigations regarding the state selection process in the flow.

In this work, an attempt is made to identify the asympotic states that can develop in laminar wakes. The investigation consists of two parts: (a) formation of vortex streets in absence of external forcing, and (b) development of asymptotic response states under periodic external forcing. The approach is that of a direct numerical simulation using the spectral-element method (Patera 1984), and (Karniadakis, Bullister & Patera 1985) a high-order, weighted residual technique, which combines the accuracy of spectral methods with the flexibility in geometry of finite-element schemes. The success of the spectral-element method in accurately resolving the fine structure of transitional flows in complex geometries in previous studies (Ghaddar *et al.* 1986; Karniadakis, Mikic & Patera 1988) recommended its use in the present investigation.

In §2 of this paper the governing equations are presented, and the spectral-element method is briefly discussed. In §3 the unforced response of laminar wakes is investigated. For a fixed value of the Reynolds number ($Re = 100$), the development of the vortex street as a function of time is followed in detail. Computer-aided flow visualizations and power-spectral-density plots are used to analyse the natural response. In §4, the response of the wake at the same Reynolds number subject to a localized in space, time-harmonic forcing is investigated. The amplitude of the forcing is kept constant, while the frequency is varied from half to three times the shedding frequency; for each case, the asymptotic state of the wake is determined by using power-spectral-density and phase-plane plots. All calculations reported in this paper have been carried out for a fixed amplitude of forcing; based on these results,

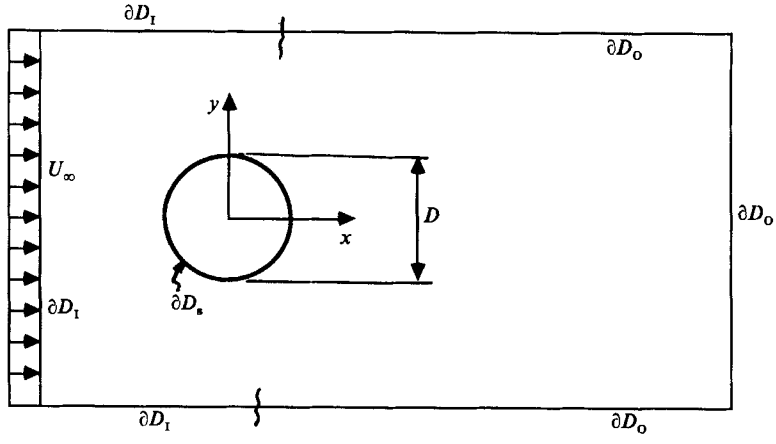

FIGURE 1. Geometry definition for flow past a cylinder in an unconfined domain.

however, we can qualitatively infer the complete form of the state-selection diagram in the amplitude–frequency plane, as discussed in §5. Finally, in §6 the implications of our results for flow-control applications are summarized.

2. Problem formulation and numerical methods

2.1. *Governing equations*

We consider here the flow past a circular cylinder in the domain depicted in figure 1, with the boundary ∂D composed of the solid walls ∂D_s, and the inflow/outflow boundaries $\partial D_I \cup \partial D_O$. A Cartesian system of coordinates is used, the origin of which coincides with the centre of the cylinder, and the axes x and y are parallel and normal to the oncoming flow respectively, with unit vectors denoted by $\hat{\boldsymbol{x}}$ and $\hat{\boldsymbol{y}}$. The governing equations for the flow are the incompressible Navier–Stokes and continuity equations,

$$\boldsymbol{v}_t = \boldsymbol{v}\times\boldsymbol{\omega} - \boldsymbol{\nabla}\Pi + Re^{-1}\boldsymbol{\nabla}^2\boldsymbol{v} + \boldsymbol{F}, \tag{1a}$$

$$\boldsymbol{\nabla}\cdot\boldsymbol{v} = 0, \tag{1b}$$

where $\boldsymbol{v}(\boldsymbol{x})\,(= u\hat{\boldsymbol{x}} + v\hat{\boldsymbol{y}})$ is the velocity, $\boldsymbol{\omega} = \boldsymbol{\nabla}\times\boldsymbol{v}$ is the vorticity, $\Pi = p + \frac{1}{2}\boldsymbol{v}\cdot\boldsymbol{v}$ is the pressure head, with p the pressure, and $Re = U_\infty D/\nu$ is the Reynolds number. Here U_∞ is the free-stream velocity, D the cylinder diameter, and ν the kinematic viscosity of the fluid. All velocities and lengths are scaled by U_∞ and by the cylinder radius R respectively. The term $\boldsymbol{F}$ on the right-hand side of (1*a*) is an external forcing, which in our investigation is a localized forcing harmonic in time, as discussed further in §4.

The boundary conditions on $\boldsymbol{v}$ for a stationary cylinder are,

$$\boldsymbol{v} = 0 \quad \text{on} \quad \partial D_s, \tag{2a}$$

$$\boldsymbol{v} \Rightarrow U_\infty \hat{\boldsymbol{x}} \quad \text{as} \quad |\boldsymbol{x}| \Rightarrow \infty, \tag{2b}$$

where ∂D_s is the cylinder surface.

Finally, in order to investigate the effects of the boundary conditions on the numerical results, periodicity conditions in the y-direction, at the sides of the computational domain, were used instead of the boundary conditions in (2*b*). This

simulation corresponded to flow past an infinite array of cylinders placed perpendicular to the flow.

2.2. *Temporal discretization*

To discretize the Navier–Stokes equations (1) in time, we use a fractional-step (splitting) method (Korczak & Patera 1986). The fractional steps involve (i) the nonlinear advection and time-dependent forcing terms; (ii) the pressure to enforce incompressibility; and (iii) the viscous terms to enforce the Dirichlet boundary condition.

The semi-discrete equations for $\boldsymbol{v}^n(\boldsymbol{x}) = \boldsymbol{v}(\boldsymbol{x}, n\Delta t)$ are then: step (i),

$$\hat{\boldsymbol{v}}^{n+1} - \boldsymbol{v}^n = \Delta t \sum_{q=0}^{2} \beta_q (\boldsymbol{v} \times \boldsymbol{\omega})^{n-q} \quad \text{in} \quad D, \tag{3}$$

followed by the pressure step (ii),

$$\hat{\boldsymbol{v}}^{n+1} - \hat{\boldsymbol{v}}^{n+1} = -\nabla \Pi \, \Delta t \quad \text{in} \quad D, \tag{4a}$$

$$\nabla^2 \Pi = \nabla(\hat{\boldsymbol{v}}^{n+1}/\Delta t) \quad \text{in} \quad D, \tag{4b}$$

$$\nabla \Pi \cdot \hat{\boldsymbol{n}} = \begin{cases} \hat{\boldsymbol{v}}^{n+1} \hat{\boldsymbol{n}}/\Delta t & \text{on} \quad \partial D_{\mathrm{s}} \quad (4c) \\ \lambda/\Delta t & \text{on} \quad \partial D_{\mathrm{I}} \cup \partial D_{\mathrm{O}}, \quad (4d) \end{cases}$$

where $\hat{\boldsymbol{n}}$ is the unit vector, normal to the boundary.

Finally the viscous corrections using a Crank–Nicolson scheme is, step (iii),

$$\boldsymbol{v}^{n+1} - \hat{\boldsymbol{v}}^{n+1} = \tfrac{1}{2} \Delta t \, Re^{-1} \nabla^2 (\boldsymbol{v}^{n+1} + \boldsymbol{v}^n) \quad \text{in} \quad D. \tag{5}$$

Here $\beta_0 = 23/12$, $\beta_1 = -16/12$, and $\beta_2 = 5/12$ are the third-order Adams–Bashforth coefficients in step (i). Also, λ is an incompressibility parameter defined as $\lambda = \iint \hat{\boldsymbol{v}} \, \mathrm{d}\boldsymbol{x} / \iint \mathrm{d}\boldsymbol{x}$ with the integration carried out over $\partial D_{\mathrm{I}} \cup D_{\mathrm{O}}$. This value of λ corresponds to a minimum adjustment required to the boundary velocity $\hat{\boldsymbol{v}}$ obtained at the end of the fractional step (i), such that the solvability condition for the pressure is satisfied. It represents a projection of the mass flux at the boundaries to an incompressible field. This projection ensures that incompressibility is enforced everywhere in the domain $D \cup \partial D$, with the $\hat{\boldsymbol{v}}$-field being projected to a divergence-free space at the domain interior D, through the $\hat{\boldsymbol{v}}$-field in the second substep.

The overall time accuracy of the scheme is dictated by the Stokes part, which has been shown (Korczak & Patera 1986) to be $O(\Delta t)$, even though the local error in each substep is of higher order. This is because the operators involved in the three substeps do not commute. Although of first order, the fractional-step scheme has the important advantage of reducing all implicit operations to uncoupled standard Helmholtz equations in steps (ii) and (iii). It is the discretization of the Helmholtz operator that we briefly discuss next.

2.3. *Spatial discretization*

For the spatial discretization of (1) we use the spectral-element method, first introduced by Patera (1984). As the fully discrete solution of the Navier–Stokes equations is given elsewhere in detail (Karniadakis *et al.* 1985; Korczak & Patera 1986) only the main points will be discussed here. In the isoparametric spectral-element method the computational domain is broken up into curvilinear quadrilaterals (elements); within each element geometry, velocity and pressure are

expanded in tensor product bases in terms of the local coordinates (r, s). In element k, we then have

$$[\boldsymbol{x}, \boldsymbol{v}, \Pi] = \sum_{i=0}^{N} \sum_{j=0}^{N} [\boldsymbol{x}, \boldsymbol{v}, \Pi]_{ij}^{k} h_i(r)\, h_j(s) = \sum_{i}^{N} [\boldsymbol{x}, \boldsymbol{v}, \Pi]_{i}^{k} g_i(r, s), \tag{6}$$

where the $h_i(z)$ are the Nth-order Lagrangian interpolants through the Gauss–Lobatto Chebyshev points and $g_i(r, s)$ are defined by (6). A recent modification of the spectral-element method employs subparametric elements with the pressure interpolated using $(N-2)$th order interpolants through Gauss–Lobatto Legendre points (Maday & Patera 1987). The choice of the collocation points is important for the accuracy of the numerical method and the collocation approximations. It has been shown (Korczak & Patera 1986), and (Rønquist & Patera 1987) that interpolations of the form of (6) result in exponential convergence for infinitely smooth solutions. Furthermore, it was shown that the weak formulation employed for global decomposition preserves the *spectral accuracy*. In spectral-element methods convergence can be obtained by two different approaches: either by maintaining the order N of the interpolants constant and increasing the number of macro-elements K, or by keeping the number of macro-elements constant and increasing the order of the interpolants, with a corresponding increase of the number of collocation points, $(N+1)$, for each element. It is the latter approach in discretization that leads to exponential convergence, whereas the former approach results in algebraic-only convergence, typical of finite-element schemes. Our numerical experiments have shown, however, that use of Chebyshev polynomials of order six or higher results in exponential convergence.

To represent the convective contributions $(\boldsymbol{v} \times \boldsymbol{\omega})$ of (1) we use a mixed collocation/Galerkin approach, and thus simply calculate the term $(\boldsymbol{v} \times \boldsymbol{\omega})$ at each collocation point (ij). For the pressure and diffusion contributions we use the standard variational formulation for second-order elliptic equations of the Helmholtz type. These equations are the result of the fractional method employed, as discussed in §2.2. The standard Helmholtz equation can be written as

$$\nabla^2 u - \alpha^2 u = 0, \tag{7}$$

where u is the unknown and α is the Helmholtz constant. We approximate (7) with its variational equivalent, i.e. the solution that minimizes the functional

$$\sum_{k}' \iint \{-\nabla_{pi}\, g_p\, g_q\, \nabla_{qj} - \alpha^2 g_i\, g_j\}\, u_j |J^k|\, \mathrm{d}\boldsymbol{x}, \tag{8}$$

where ∇_{ij} is the discrete gradient operator, J^k is the Jacobian of the transformation, and Σ_k' denotes direct stiffness summation over elemental interfaces.

A static condensation algorithm is employed to solve the resulting system (Korczak & Patera 1986). This greatly reduces the order of the system, and decouples the unknowns at the elemental nodes from those in the interior of the element.

The spectral-element method is a technique particularly appropriate for direct simulations of unsteady and transitional flows, owing to its rapid (exponential) convergence, good resolution properties, and minimal numerical dispersion and diffusion. A typical spectral-element mesh used in our calculations is shown in figure 2. Very high resolution is placed around the cylinder in order to accurately compute the boundary layer. Notice that the cylindrical geometry is represented exactly, as isoparametric expansions are employed to map the curvilinear elements onto

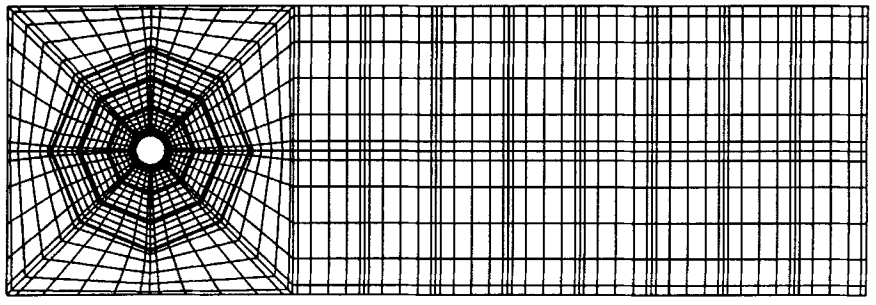

FIGURE 2. A typical spectral-element mesh. Small size elements are used close to the cylinder to obtain high resolution, whereas larger elements are used further downstream.

standard squares; the latter represent spectral elements in a 'local' reference frame. Therefore, in order to determine the coordinates of all collocation points $\boldsymbol{x}_{ij}$ in the physical mesh, we first specify the coordinates $\boldsymbol{x}_{ij}$ along all curvilinear boundaries according to Chebyshev distribution in arclength. Once the elemental coordinates are known, the remaining interior points for each element are determined by deforming the local (r, s) mesh into its (x, y) image using 'uniform strain' techniques (Korczak & Patera 1986).

The boundary conditions on the computational mesh are taken to be uniform oncoming flow, potential flow at side 'walls', no-slip on the cylinder walls, and outflow Neumann conditions ($\partial \boldsymbol{v}/\partial \boldsymbol{n} = 0$, where $\boldsymbol{n}$ denotes normal to the boundary direction) at the downstream boundary. Various experiments were carried out to verify the mesh-independence of the solution, and different boundary conditions at the truncation of the infinite domain were employed. In particular, for the mesh shown in figure 2 the order of the Chebyshev polynomials, N, was increased from six to eight resulting in an increased total number of collocation points from 2744 to 4536. There was no change in the frequency of the nonlinear response, while the amplitude of the oscillation was found to differ less than 1%. Simulations using a similar mesh to that in figure 2, but twice as wide (forty cylinder diameters wide) were repeated for one case of $Re = 100$, and the frequency was found to decrease by 1%, while the difference in the amplitude of the oscillations was less than 2%. Furthermore, the replacement of Dirichlet boundary conditions at the sides of the domain with periodic boundary conditions had no detectable effect on the solution.

The time-step is essentially imposed by the numerical stability required for the first substep that treats explicitly the advection terms. In most of the simulations presented here, the time-step Δt was equal to 0.018 time-units. Given that for Reynolds number $Re = 100$ the period of oscillation τ is equal to 11.2 time-units, the time-step we have used gives a resolution of 622 time points per period of oscillation. All computations were performed in a CRAY X-MP/48. A typical computational index for our simulations is $\tau_c = 7 \times 10^{-5}$ in CPU s/(time-step·node), utilizing a single processor. This cost is essentially dictated by the static condensation algorithm employed to solve the system global matrix for all elemental boundary nodes; the operation count is estimated as $O(K^3N^2)$, where K and N are the number of elements and the order of the Chebyshev polynomials used respectively. This cost can further be reduced, by using a K^2-headed processor machine, to an operation count of $O(K^2N^2)$.

Last, we note that a similar code as the one employed in the current study has been used in many past investigations in which exhaustive comparisons with experimental

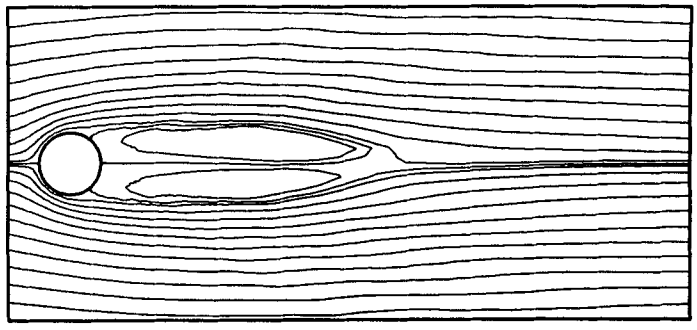

FIGURE 3. Streamline pattern showing the onset of oscillation at $Re = 100$; non-dimensional time $t = 72$.

and empirical data have been performed (Karniadakis 1988; Karniadakis, Mikic & Patera 1988).

3. Response of unforced wakes

In this Section, the development of the vortex street in an unforced laminar wake at Reynolds number 100 is studied. The uniform flow upstream of the cylinder is 'switched-on' at time $t = 0$, and then, after a steady periodic state is reached, the flow is simulated over a period of time (typically, twenty flow cycles), sufficient to obtain reliable estimates of the power spectral density of the velocity fluctuations. Computer-aided flow visualizations have been used to study the space–time development of the vortex street. The results are discussed below in detail.

In the early stages of the flow, a quasi-steady separated flow develops, characterized by the formation of the 'separation bubble', i.e. a region of recirculating flow, behind the cylinder. The length of the separation bubble increases with time in a manner similar to that at subcritical Reynolds numbers (Karniadakis 1988), but at a faster rate. When it reaches approximately the length predicted by a steady-flow type of analysis, with forced flow symmetry (Fornberg 1985), the onset of an oscillation can be seen through the breaking of symmetry of the flow (figure 3). From there on, the oscillation grows in time and spreads in space, leading eventually to the formation of the vortex street. Different stages in the development of the vortex street are shown in figure (4*a–d*).

After the formation of the vortex street, the *time-average* flow field has been computed (figure 5). The time-average flow field is similar to the initial one, but with the important difference that it has a separation bubble of length much smaller than the initial one, shown in figure 3. This shows that the average flow field is influenced by the development of the vortex street, and is drastically different from the initial quasi-steady flow field. The difference can be attributed to the fact that the Reynolds stresses produced by the vortex street cause, through increased momentum transfer, a higher 'apparent viscosity' in the flow, or, equivalently, a lower effective Reynolds number. Consistently with this interpretation, the flow behind the cylinder, where the vortices are still forming, is less influenced than the flow further away, where the vortices have grown to their final size. This can be seen more clearly in figures 6 and 7, where the time-average velocity profiles at different x-locations in the near wake *before* the formation of the vortex street are compared with the ones *after* the formation. The most obvious difference between the two can be seen in the variation of the centreline velocity along the x-direction.

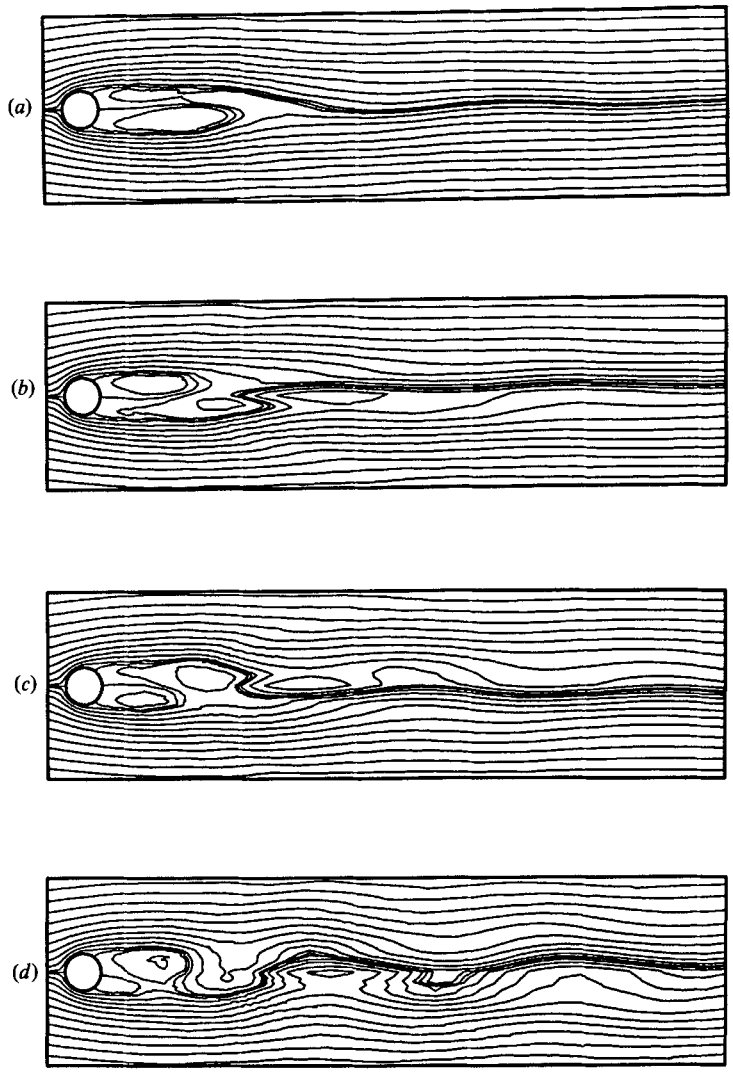

FIGURE 4. Instantaneous streamlines showing the evolution of the vortex street after symmetry is broken. The corresponding times are (*a*) $t = 90$; (*b*) 99; (*c*) 112.5; (*d*) 135.5.

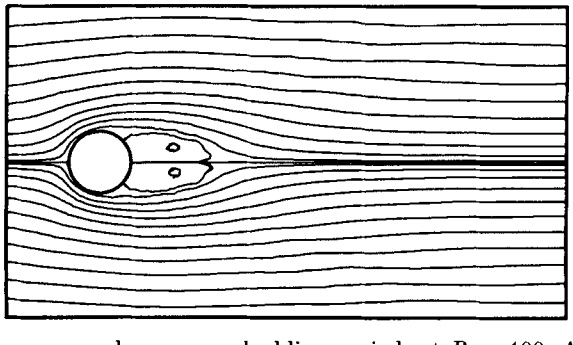

FIGURE 5. Streamlines averaged over one shedding period, at $Re = 100$. A significantly smaller wake bubble is shown than the initial one (figure 3) or the computed steady patterns of Fornberg (1985).

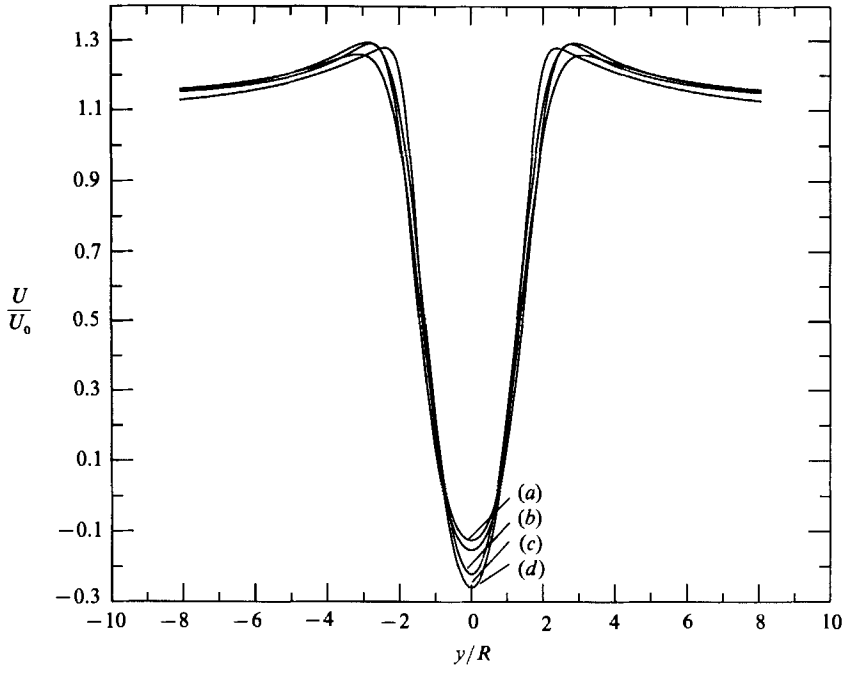

FIGURE 6. Velocity profiles of the initial flow at different locations. Curve (*a*) $x = 2$, (*b*) 3, (*c*) 4, (*d*) 5. The magnitude of the centreline velocity increases with x, reaching its maximum at $x = 5$.

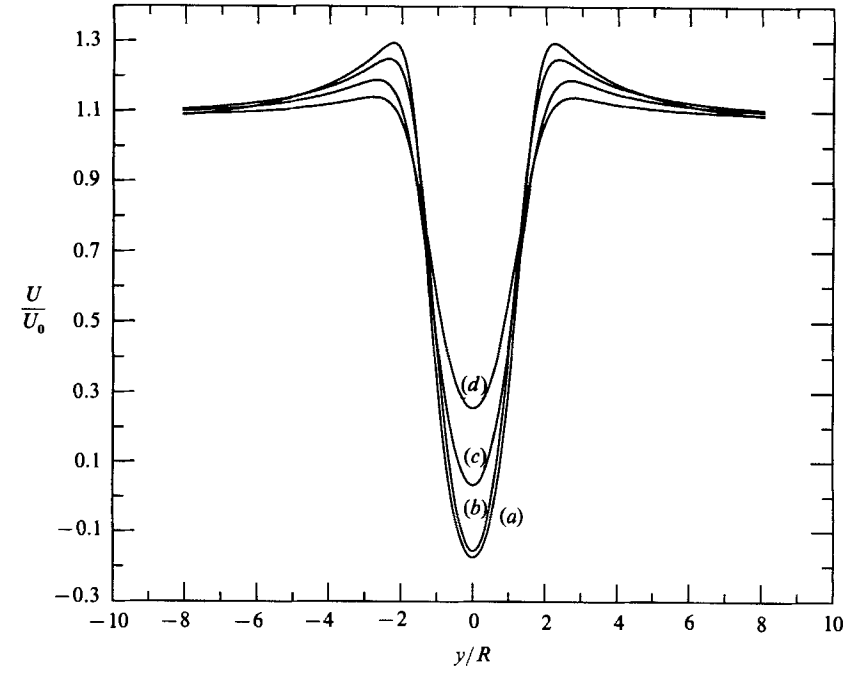

FIGURE 7. Velocity profiles of the average flow at different locations. Curve (*a*) $x = 2$, (*b*) 3, (*c*) 4, (*d*) $x = 5$. The magnitude of the centreline velocity decreases as x increases.

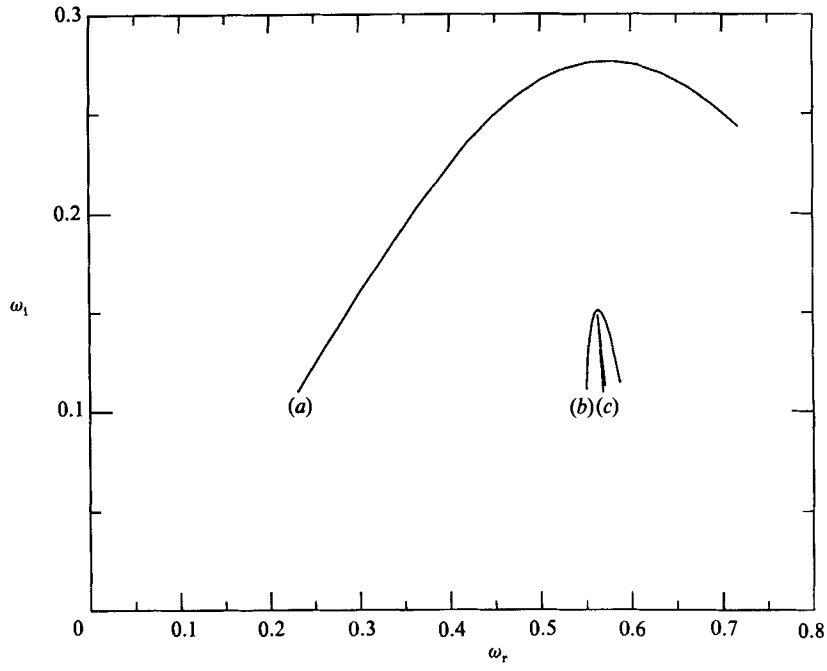

FIGURE 8. Map of lines k_i = constant in the ω-plane for the profile of the average flow at $x = 2$ and $Re = 100$. Curve (*a*) $k_i = 0$, (*b*) -0.40, (*c*) -0.463. The 'pinch-point' lies at the cusp of curve (*c*). Note, $St = \omega_r/\pi$.

A linearized stability analysis of the *time-average* flow has been performed, by assuming that the latter is slowly varying in the x-direction. This is supported by the form of the velocity profiles in figure 7. The stability of the wake can then be analysed separately at each location along the wake assuming a locally parallel flow. A discussion of non-parallel flow effects, based on a Ginzburg–Landau model, can be found in Chomaz, Huerre & Redekopp (1988). The physical character of the wake instability has been investigated, i.e. whether the instability is absolute or convective. The instability in an infinite medium is termed absolute if any arbitrary disturbance grows in time at any fixed location in space, or convective if disturbances are convected away from the point of excitation leaving the medium undisturbed (Bers 1983). Within linear theory, the distinction between the two types of instability in a homogeneous medium can be made from the dispersion relation $D(\omega, k) = 0$ of the medium, where ω is the frequency and k the wavenumber. More specifically, the 'pinch-point' type of double-root of the dispersion relation (Bers 1983) with the largest imaginary part determines the character of the instability. If the latter gives a complex frequency with a positive imaginary part, the instability is absolute, and the real part of the pinch-point frequency gives the 'preferred frequency' of the instability. If the imaginary part is negative, the instability is convective.

The dispersion relation consists of the Rayleigh equation, subject to the condition that the perturbation velocity vanishes at the 'sidewalls' of the domain. The pinch-point was determined using the method suggested in Triantafyllou, Triantafyllou & Chryssostomidis (1986), and Triantafyllou, Kupfer & Bers (1987). In this method, the complex wavenumber plane is mapped into the complex frequency plane through

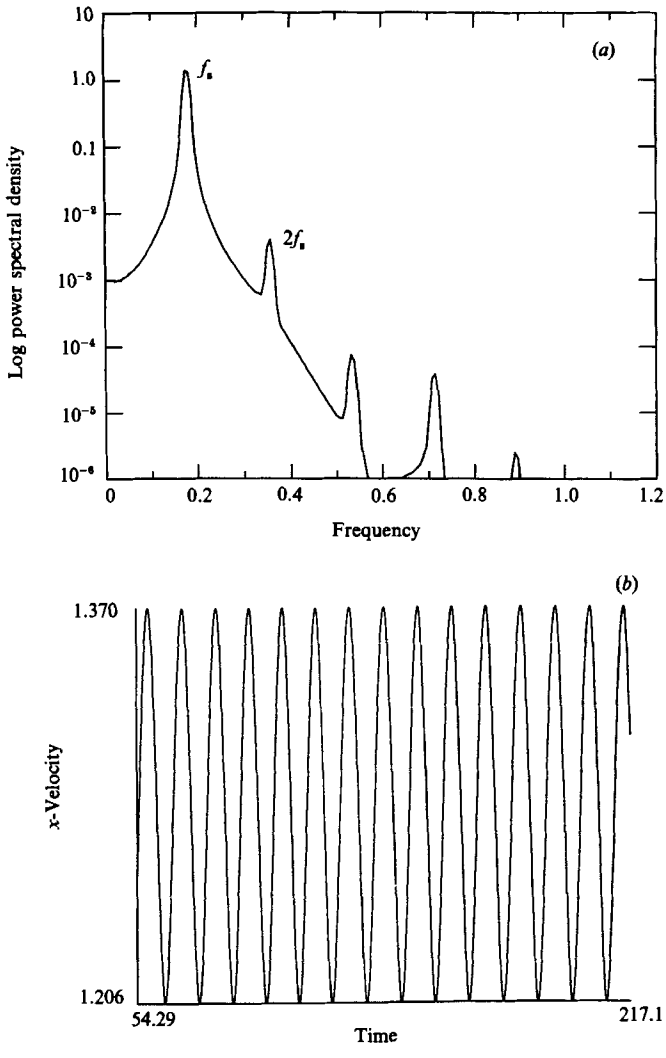

FIGURE 9. A typical power spectrum (*a*) and corresponding time trace (*b*) for a point located at ($x = 2.0$; $y = 2.0$), at $Re = 100$, without external forcing. Only the shedding frequency, f_s, and its superharmonics are present in the spectrum.

the dispersion relation; the location of double roots of the dispersion relation can then be identified through the similarity of the map to the mapping of the quadratic function (figure 8). The requirement that the double root be of the pinch-point type can be verified from the location of the double root relative to the map of the k-real axis in the complex frequency plane. The latter, curve (*a*) in figure 8, is intersected by the line perpendicular to the ω-real axis passing through the double root only once. Consequently, the reverse mapping of this vertical line into the k-plane through the dispersion relation will intersect the reverse mapping of curve (*a*), i.e. the k-real axis, only once, satisfying the 'pinching' condition (Triantafyllou *et al.* 1987).

The average flow is *absolutely unstable* over a region of approximately 5 radii behind the cylinder; the rest of the wake is convectively unstable. Therefore, the absolute instability of the average flow in the near wake sustains the vortex street,

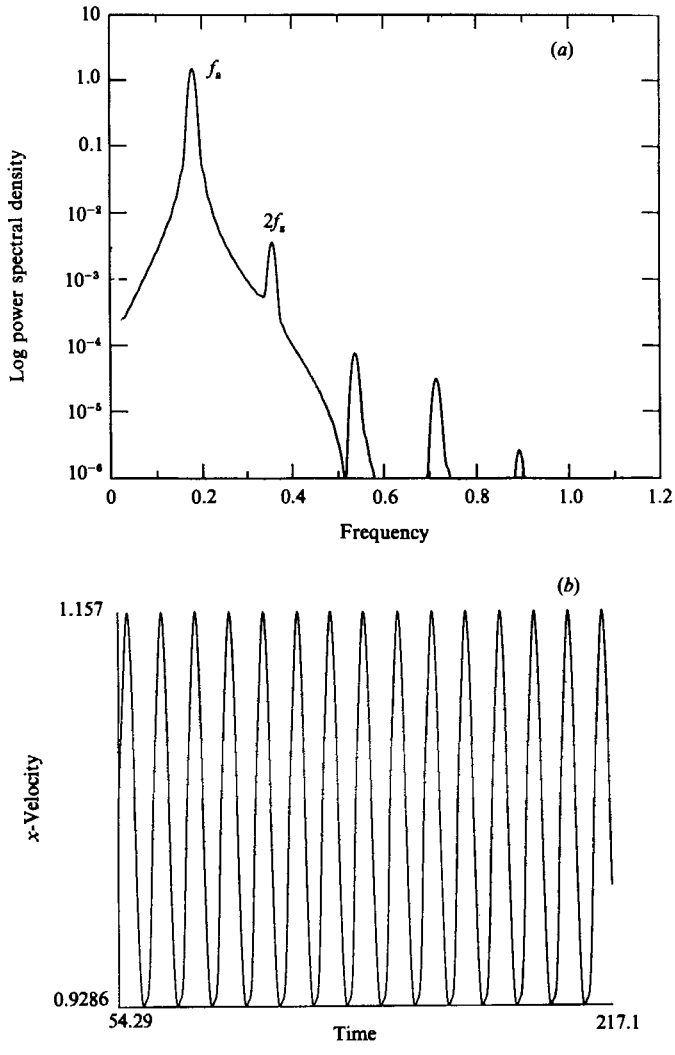

FIGURE 10. Power spectrum (*a*) and time trace (*b*) for natural shedding at $Re = 100$ showing a periodic state. The point traced is located at ($x = 20$; $y = 2.0$), close to the point where Sreenivasan (1985) reported chaotic behaviour.

as found by Triantafyllou *et al.* (1986) by analysing the stability of the experimentally measured average flow behind circular cylinders at representative Reynolds numbers. The quantitative agreement between the numerical calculation and the stability analysis is excellent: the Strouhal number predicted by the direct simulation is equal to 0.179, and the 'natural frequency' found from the stability analysis of the 'most unstable profile', located at $x = 2$, also gives a value equal to 0.179 (figure 8). We note that the instability of the most unstable profile ($x = 5$) of the initial average flow, *before* the establishment of the vortex street, predicts a Strouhal number equal to 0.13, which accurately describes the oscillation frequency in the initial stage of the flow only. Consequently, we can conclude that the initial quasi-steady flow, which initiated the formation process, has been lost from the picture. It is the absolute instability of the *final average flow* that sustains the oscillation in the wake, by feeding energy into it in the near wake. The success of the *linear* theory, may be

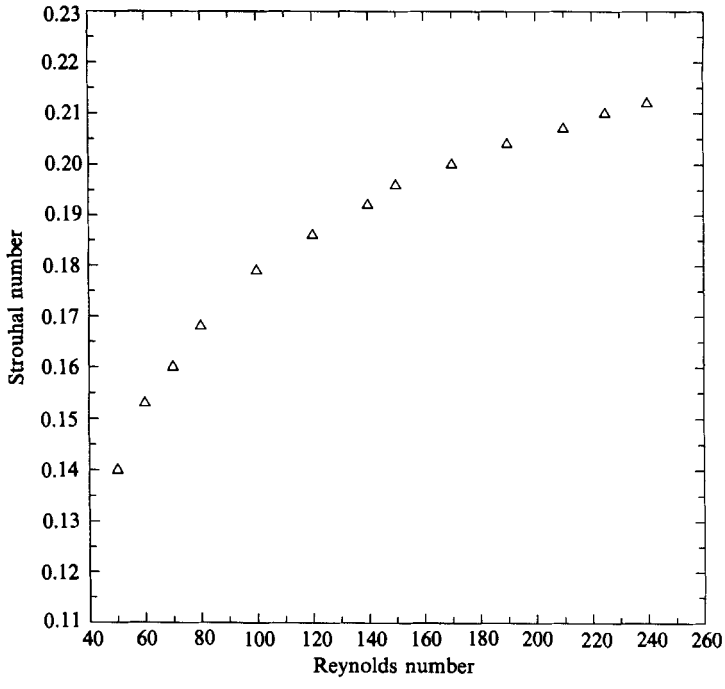

FIGURE 11. Plot of the relationship between the Strouhal and Reynolds numbers for the natural shedding response. No discontinuities are shown in the curve, contrary to the experimental results reported, first, by Tritton (1959).

attributed to the fact that the velocity fluctuations about the average value are relatively small; this can be verified from the time traces in figures 9(*b*) and 10(*b*). In the near wake (figure 9*b*), the fluctuations are about 8%, and in the far wake (figure 10*b*) 11% of the free-stream velocity.

For Reynolds number equal to 100, Roshko's (1954) empirical formula gives a Strouhal number equal to 0.167. The Strouhal number predicted by our numerical calculation is thus higher than the experimental one by about 8%. In order to investigate this discrepancy, we first tested the accuracy of the calculations by using a spectral-element mesh with much higher resolution; the new mesh yielded the same results. We thus concluded that for the computational domain shown in figure 2 our calculations were accurate; this is further supported by the excellent agreement obtained with the results of the stability analysis of the time-average flow. Next, in order to investigate the effect of the size of the domain on the value of the Strouhal number, we repeated the calculation with a different mesh, twice as wide as the one in figure 2. In the new calculation, the Strouhal frequency was reduced by 2%. The disagreement between our numerical computations and Roshko's (1954) experiments can, therefore, be partly attributed to the truncation of the computational domain in our numerical simulations, which causes an increase in the Strouhal number (Chilukuri 1987). However, errors may be present in the experimental measurements too, introduced by the three-dimensionality of the flow; this has been pointed out by Friehe (1980), who has shown that the Strouhal frequency is reduced significantly as the aspect ratio (cylinder length/cylinder diameter) decreases. We also note that our computed value of the Strouhal number is in total agreement with the one computed by Gresho *et al.* (1984) using a finite-element method.

The vortex street at Reynolds number 100 is an almost harmonic oscillation, as attested by the time trace and the power spectral density of the velocity fluctuations. This can be seen in figure 9(*a*, *b*), for the point with coordinates ($x = 2, y = 2$) in the near wake, and in figure 10(*a*, *b*) for the point ($x = 20, y = 2$) in the far wake; for both points the velocity component in the x-direction has been analysed. The point at the far wake has been chosen close to the location where chaotic behaviour was reported by Sreenivasan (1985), at a Reynolds number lower than ours. No evidence of chaos can be detected in our results (we tested several other locations along the wake, not shown here). In that respect, our simulations support the conclusions of Van Atta & Gharib (1987), that the asymptotic state in unforced laminar wakes is always periodic.

Based on our results about the frequency selection process in laminar wakes, discontinuities in the relationship between the Strouhal and Reynolds numbers of the *two-dimensional flow*, as found by Tritton (1959) seem unlikely; as a further test, we calculated the unforced response of the wake for several Reynolds numbers ranging from 40 to 250. The numerical results (figure 11), show indeed a continuous variation of the Strouhal number with the Reynolds number.

4. Response of forced wakes

4.1. *Asymptotic states*

In this section the forced response of the wake to a time-harmonic forcing is investigated. Within linear theory, an absolutely unstable flow, like the wake of the cylinder, is not receptive to external forcing: the naturally produced instability wave grows exponentially in time, whereas the forced wave is oscillatory in time. As a result, the naturally produced wave becomes exponentially larger than the forced wave and completely dominates the response. This conclusion, however, is only valid if the amplitude of the forcing is infinitesimal. Finite-amplitude forcing can make its presence felt through nonlinear effects. There is therefore a 'threshold amplitude' above which the forced wave becomes visible, as found experimentally by Koopmann (1967) for the low-Reynolds-number wakes behind vibrating cylinders (see also the discussion in Berger & Wille 1972). Once the 'threshold amplitude' has been exceeded, the naturally produced periodic state may lose its stability, leading to the development of non-periodic states. The response states resulting from a time-periodic forcing at an amplitude larger than the 'threshold' are discussed in this section.

The forcing used is an acceleration harmonic in time and localized in space, described by the equation

$$F(x, y, t) = A \cos(2\pi f_e t) \exp(-\tfrac{1}{16}((x-2)^2 + y^2)), \tag{9}$$

where A is the amplitude of the acceleration and f_e is the frequency. The idea behind the choice of this type of forcing was to simulate the localized excitation provided by an active control device in the near wake of the cylinder, like, say, a thin vibrating wire. The vibrating wire provides such a forcing through its added-mass effect: the fluid particles adjacent to the wire acquire an acceleration equal to that of the wire; further away from the wire, the acceleration of the fluid particles is gradually reduced to zero. Thus the forcing of the vibrating wire is simulated, at least qualitatively, by (9). Furthermore, vibrations of the cylinder give rise to a similar forcing. If we formulate the problem in a frame of reference that moves with the cylinder, we obtain the Navier–Stokes equations with a forcing equal everywhere to

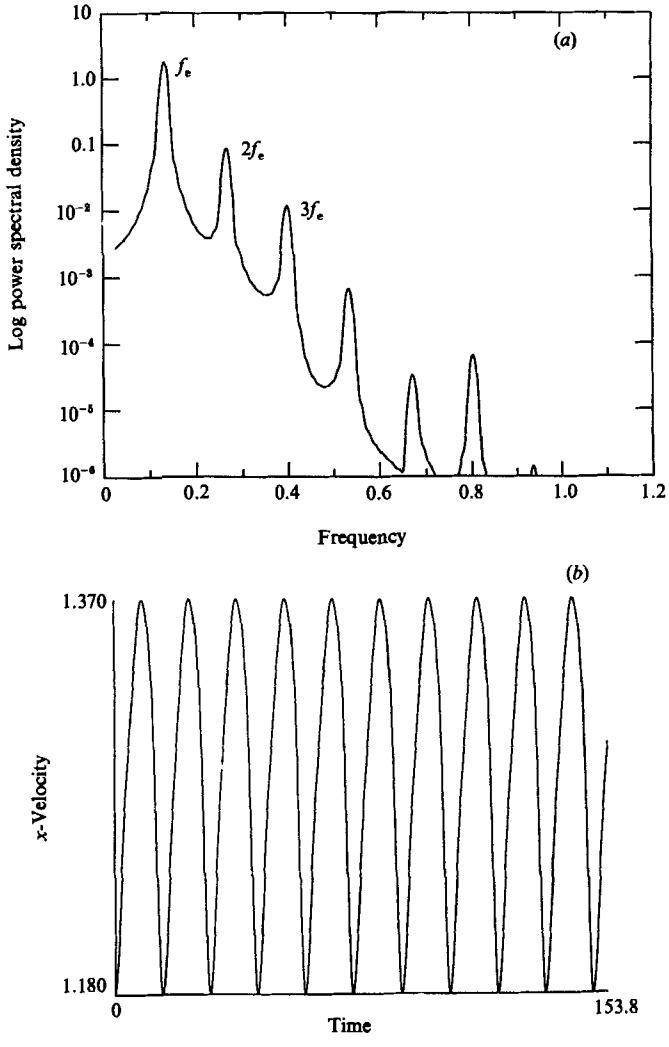

FIGURE 12. Power spectrum (*a*) and time trace (*b*) of forced response at $f_e = 0.75f_s$ at a near-wake point ($x = 2.0$; $y = 2.0$): periodic lock-in state.

the acceleration of the cylinder (with a minus sign). The forcing in (9) can therefore alternatively be thought of as *spatially truncated* version of the forcing caused by the cylinder vibrations.

The amplitude, A, of the forcing in (9) is kept constant (equal to 0.10), whereas the frequency f_e is varied, from one half to three times the natural shedding frequency. For each case, the unforced response is used as initial condition, and the computation is carried on until an asymptotic state is reached; the frequency content of the response is then determined by calculating the power spectral density of the velocity fluctuations at various locations along the wake. The forcing function in (9) attains its maximum at the point ($x = 2, y = 0$) in the near wake, and provides a forcing of significant value throughout the near wake, a condition that we found necessary for the effectivenes of any localized forcing. Consequently, the forcing excites a wave *in* the near wake that competes with the naturally produced one. The final state of the wake results from the interaction of these two waves, and depends on their

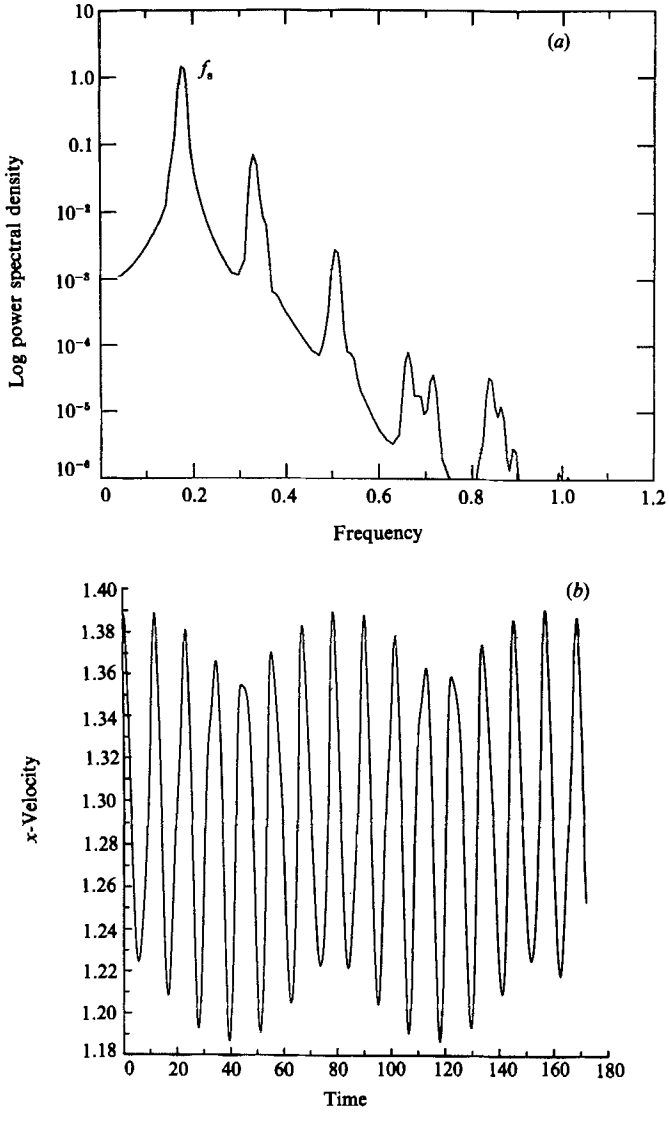

FIGURE 13. Power spectrum (*a*) and time trace (*b*) of forced response for $f_e = 1.85f_s$ in the near wake: quasi-periodic state with peak frequency f_s.

comparative importance. By varying the frequency f_e over the receptivity range of the wake, the possible response states can be identified.

Our results demonstrate that, depending on the dominant frequency of the response, there can only be two possible response states in the wake: (*a*) a lock-in state, in which the dominant frequency equals the excitation frequency, or (*b*) a non-lock in state, in which the dominant frequency equals the natural shedding frequency. The time trace and power spectral density of a lock-in state are shown in figure 12(*a*, *b*) for the near wake, corresponding to an excitation frequency $f_e = 0.75f_s$. The lock-in state is similar to the unforced one, in that the spectral density peaks only at the dominant frequency and its superharmonics, although the latter are considerably more pronounced than in the unforced state. Spectra plots and time traces obtained at several other points along the wake show the same pattern.

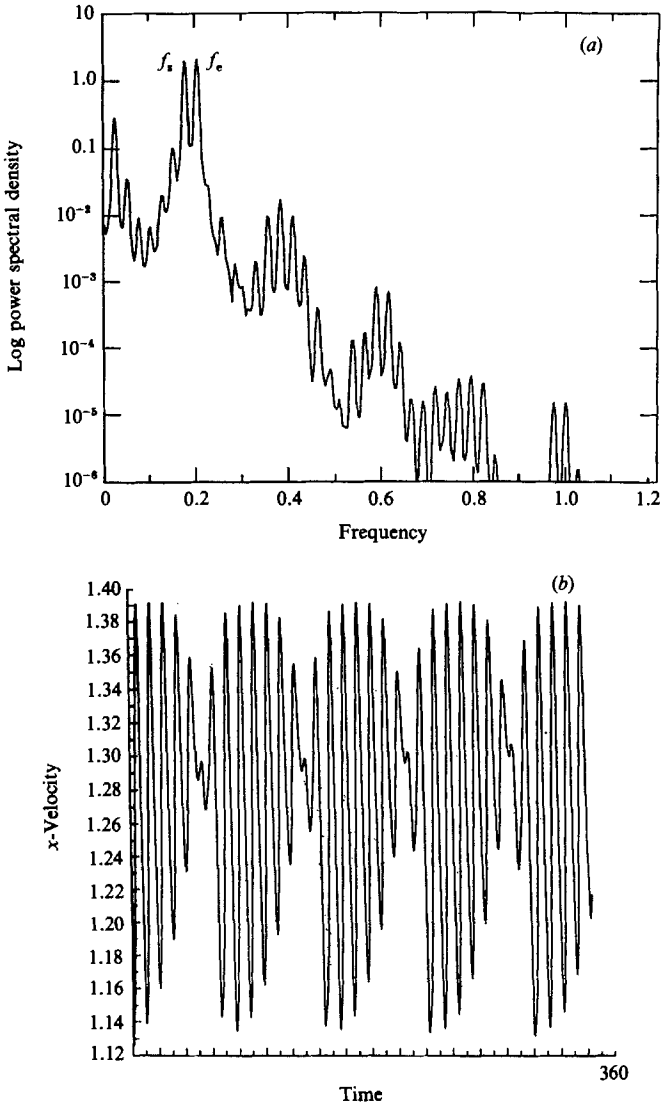

FIGURE 14. Power spectrum (*a*) and time trace (*b*) of forced response at $f_e = f_b = 1.15f_s$ in the near wake. The length of the time signal is 343.80 time units. A sudden broadening of the spectrum and loss of periodicity in the trace coincides with the appearance of two equal peaks at frequencies f_s and f_e.

In a non-lock-in state, the dominant frequency equals the natural shedding frequency; several other frequencies, however, may also be present, resulting from the nonlinear interaction between the natural and the forced waves. In figure 13(*a*, *b*) the time trace and power spectral density of the response as shown for the near wake for an excitation frequency $f_e = 1.85f_s$. The dominant peaks occur at the natural shedding frequency and its superharmonics, although the presence of some other, rather weak, peaks can also be seen. As f_e is reduced towards f_s, the peak of the spectral density at f_e becomes more and more pronounced, with the number of peaks also increasing, indicating distribution of energy over a larger number of modes.

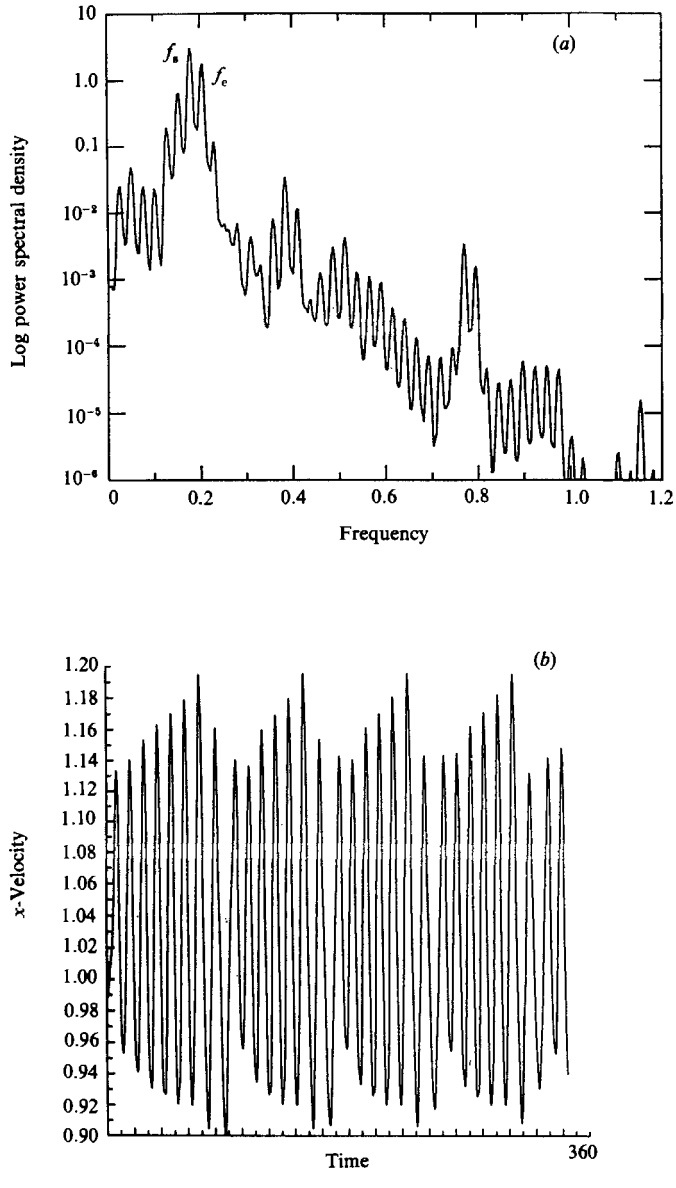

FIGURE 15. Power spectrum (*a*) and time trace of forced response at $f_e = f_b = 1.15 f_s$ in the far wake. The spectrum contains a very large number of peaks. The peak at the natural frequency slightly exceeds the peak at f_e. The signal analysed was 343.80 time units long, recorded after all transients had disappeared.

From the results presented so far, we can expect that the boundary frequency, f_b, separating the two different responses should be characterized by the presence of two equal peaks of the spectral density, at f_e and f_s. This is very nearly achieved at the near wake when $f_e = 1.15 f_s$, as shown in figure 14 (*a*, *b*), where the power spectral density and time trace at the near wake are shown; for the far wake they are shown in figure 15 (*a*, *b*). At this excitation frequency, the overall form of the power spectral density is indicative of a low-order chaotic response. A unique feature of the response at this excitation frequency is that the vortex-shedding frequency is *not constant*, but

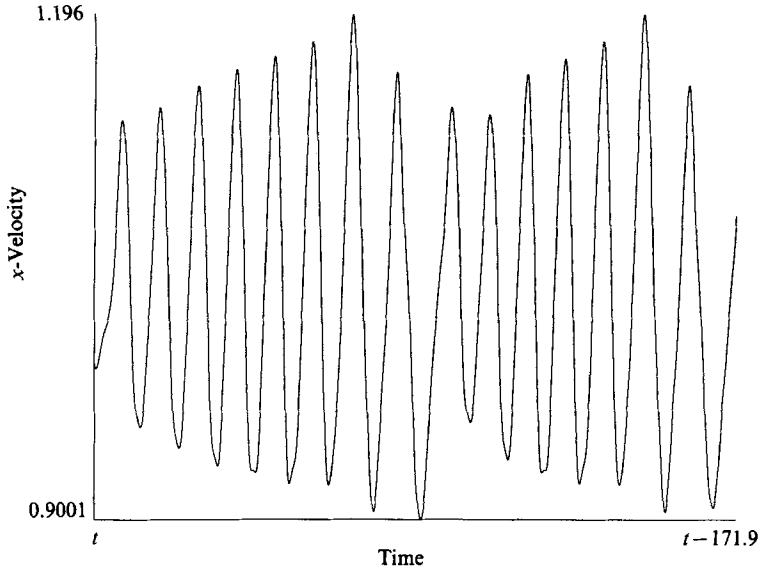

FIGURE 16. Magnified plot of the time trace at the far-wake point, showing a continuous variation of the frequency from the natural frequency f_s to the excitation frequency f_e.

varies between f_e and f_s (figure 16). Vortex shedding at alternating frequencies at the boundary of the lock-in state has been observed experimentally by Stansby (1976), for the similar problem of a mechanically vibrated rigid cylinder in steady flow. More recently, Van Atta & Gharib (1987) have shown that chaotic states in laminar wakes are characterized by a 'mode uncertainty' behaviour: the spectra of short-time signals from the wake taken at different times exhibit different dominant frequencies (figure 11 in Van Atta & Gharib 1987); this behaviour is the same as the one we report here. From our results it follows that when the excitation frequency f_e is slightly lower than f_b, the peak of the spectral density plot at f_e slightly exceeds the one at f_s. This is actually the case for the near-wake spectrum of the forced response at $1.15f_s$ in figure 14(*a*). Conversely, when f_e is slightly higher than f_b, the peak at f_s exceeds the one at f_e. This is the case for the far-wake spectrum of the same response (figure 15*a*). This implies that the exact value of the boundary frequency f_b varies along the wake, and, consequently, that transition between the two different types of response occurs for slightly different frequencies at different locations in the wake. A narrow frequency range is thus defined over which the wake develops a chaotic response. For excitation frequencies inside this range, the distinction between lock-in and non-lock-in breaks down, since lock-in and non-lock-in states coexist at different parts of the wake. This further supports the concept of 'mode uncertainty' in the wake.

For excitation frequencies outside this range, a more ordered response is recovered. Thus, for $f_e = 1.20f_s$, a quasi-periodic non-lock-in state is established, with a spectral-density plot that still shows a fairly rich frequency content (figure 17). In figure 18, the spectral density for $f_e = 1.40f_s$ is shown, which is indicative of an even more ordered motion. For frequencies below f_b, a periodic lock-in state is quickly established; this can be seen in figure 19, corresponding to $f_e = 1.10f_s$ (although some low-frequency modulation can still be detected). For f_e/f_s between 1.10 and 1.15 intermediate types of response develop. Consequently, transition from lock-in to

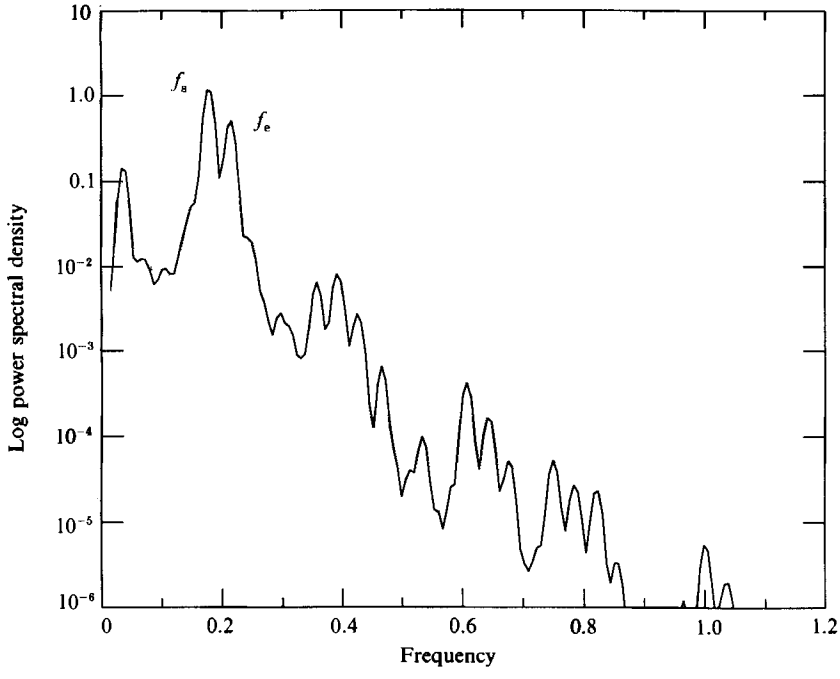

FIGURE 17. Power spectrum of forced response at $f_e = 1.20f_s$. Although the spectrum is still rich in frequency content, the response is ordered, unlike the one obtained when $f_e = 1.15f_s$.

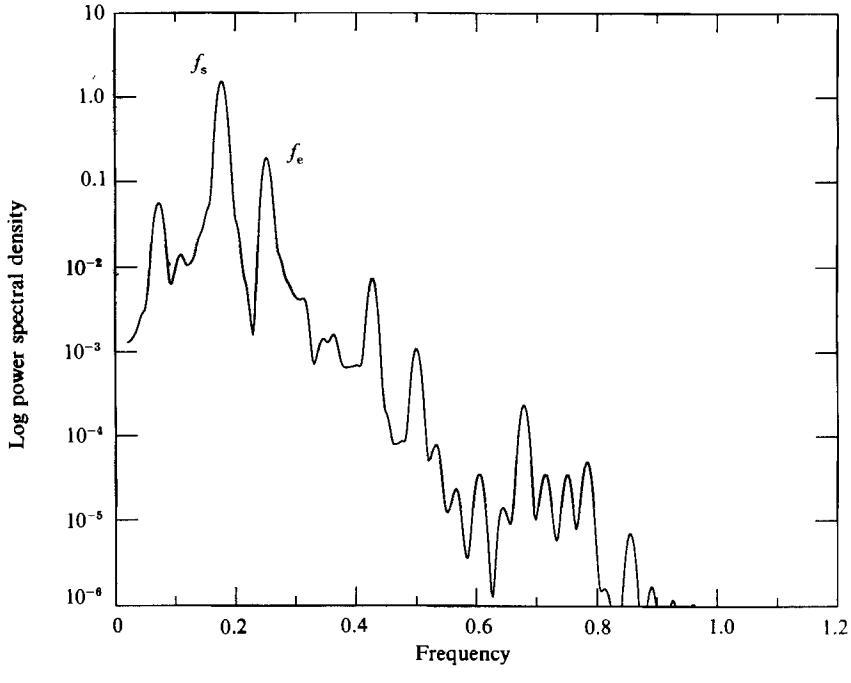

FIGURE 18. Power spectrum of forced response at $f_e = 1.40f_s$. As the excitation frequency further deviates from the 'transitional' frequency f_b the response becomes more ordered.

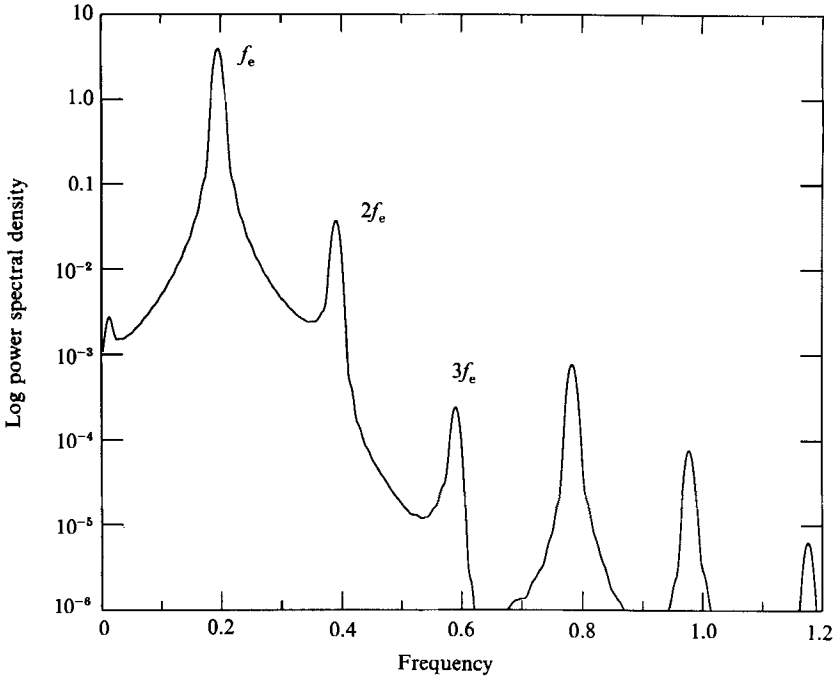

FIGURE 19. Power spectrum corresponding to a periodic lock-in state; $f_e = 1.10f_s$.

non-lock-in states as a function of the excitation frequency occurs in a continuous, even though fast, manner.

Finally, when the excitation frequency exceeds the value of $2f_s$, the effect of the excitation frequency on the response spectrum becomes negligible. This indicates that, for the amplitude used in our calculations, the upper end of the receptivity region of the wake is reached. No attempt has been made to determine precisely the lower end of the lock-in and the receptivity region, owing to the high cost of low-frequency computations. A qualitatively similar behaviour is anticipated.

4.2. *Phase-plane analysis*

The different responses have been analysed using phase–plane techniques. If we think of the cylinder wake as a high-order autonomous system under forcing, phase-space analysis can be used to characterize its response. In order to obtain a geometrical picture of the system response we 'projected' the trajectory of the system onto the two-dimensional space defined by two arbitrary independent state variables of the system. The two independent quantities that we selected are the streamwise and the vertical components of the velocity vector at the point ($x = 2.0$; $y = 2.0$). This point lies in the near wake close to the upper row of vortices of the vortex street. The choice is consistent with our finding that the state selection occurs in the near wake.

Periodic states are characterized by a limit-cycle type of behaviour in the phase plane, i.e. a closed trajectory traced continuously in time. Such a behaviour is demonstrated in figure 20 for a periodic lock-in response, corresponding to excitation frequency $f_e = 1.10f_s$. At the boundary frequency, $f_b = 1.15f_s$, the trajectory becomes aperiodic, indicative of strange (chaotic) behaviour, as shown in figure 21. This plot can be compared with the chaotic pattern discovered by McLauglin & Orszag (1982),

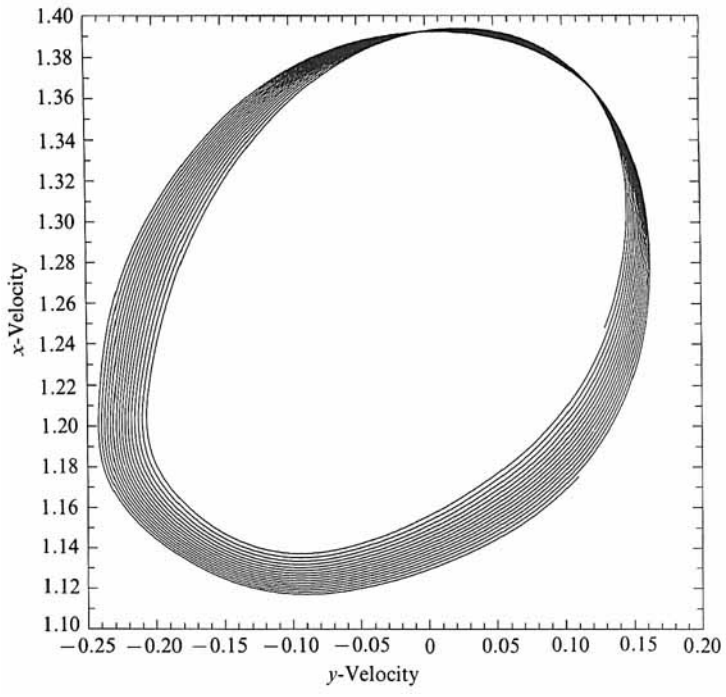

FIGURE 20. Phase portrait of the lock-in state at $f_e = 1.10 f_s$. This state marks the boundary between pure lock-in limit cycles and modulated lock-in responses.

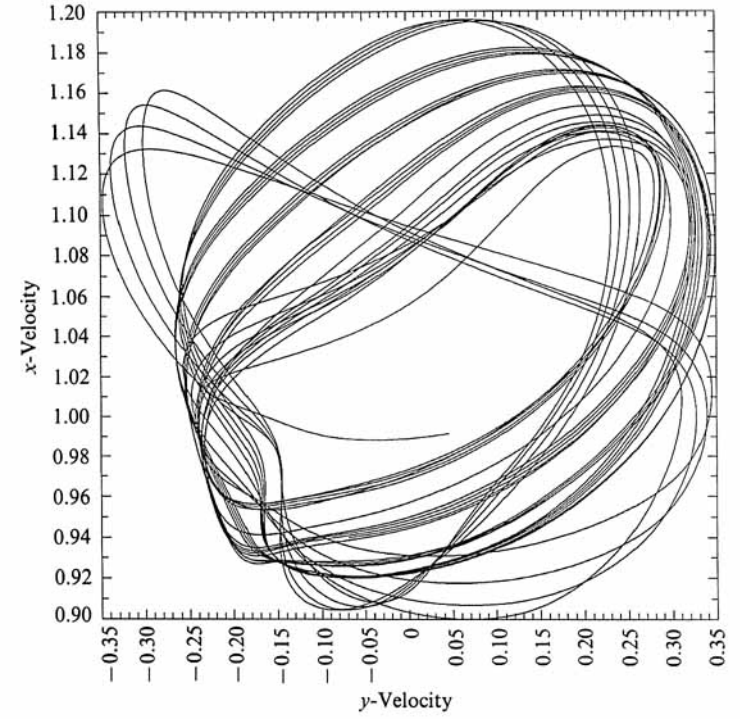

FIGURE 21. Phase portrait of the transitional state at $f_e = f_b = 1.15 f_s$. Similar portraits were obtained for very high-resolution simulations verifying that this response is independent of the discrete properties of the system.

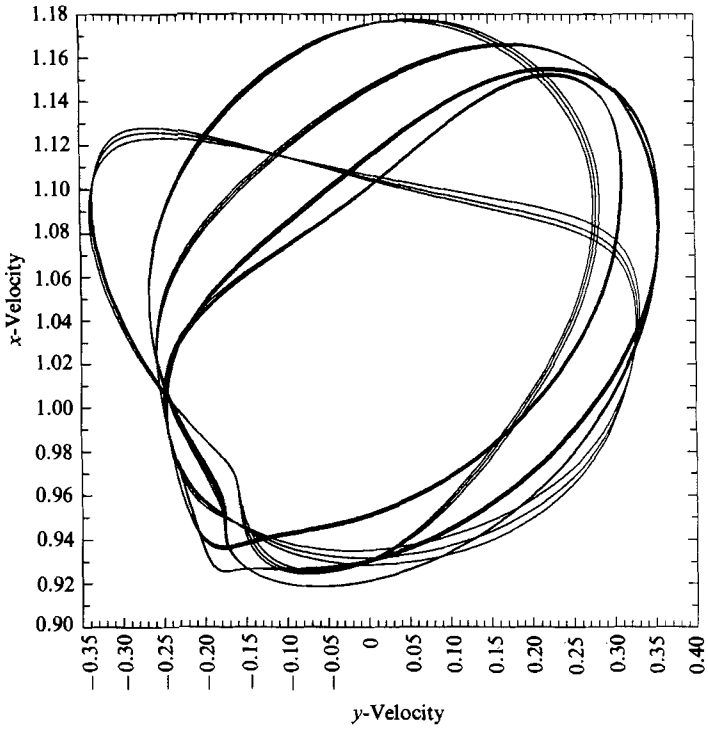

FIGURE 22. Phase portrait corresponding to a quasi-periodic state (figure 17).

shown in their figure 10. For $f_e = 1.2f_s$, a more ordered state is recovered, characterized by a quasi-periodic orbit (figure 22). Finally, at even higher f_e, limit-cycle behaviour is eventually recovered.

4.3. *Spatial structure*

Phase-plane type of analysis of flow patterns, although very useful in the identification of the temporal development of the flow, does not reveal anything about its spatial structure. The spatial structure deserves separate consideration, because it is also characteristic of the state of the flow. In this Section, an attempt is made to relate the spatial structure of the wake to the state of the flow. This is done by looking at the wavelength of the vortex street for three representative response states.

In the unforced wake, the wavelength of the vortex street varies slowly along the wake, as shown in figure 23(*a*); the wavelength is equal to, approximately, 5 cylinder diameters in the near wake, and is slowly decreasing downstream, in the far wake. In periodic non-lock-in states, the same spatial structure of the vortex street is observed. In periodic lock-in states, however, the wavelength of the vortex street changes, and can become quite different from that of the unforced state. This can be seen most clearly for the case $f_e = 0.75f_s$: the wavelength at the near wake is equal to 7 cylinder diameters, as shown in figure 23(*b*), corresponding to an increase of about 40% over the natural state. A similar change in the spatial structure of the vortex street is observed in all periodic lock-in states considered. Interestingly, the *phase velocity* of the vortex street, defined as the ratio of the dominant frequency in the wake over the wavenumber at each location in space, remains approximately the

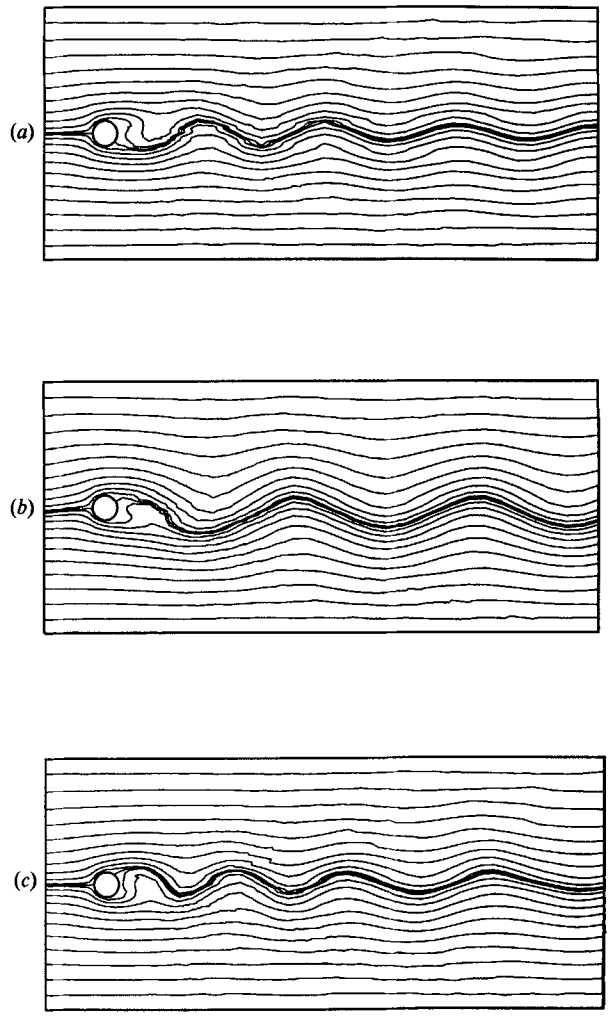

FIGURE 23. (*a*) Instantaneous streamlines at $Re = 100$ for natural shedding. The wavelength of the vortex street is approximately five diameters. (*b*) Instantaneous streamlines at $Re = 100$ and excitation frequency, $f_e = 0.75 f_s$ (a lock-in state). The wavelength of the vortex street is approximately seven diameters. (*c*) Instantaneous streamlines at the transitional state, $f_b = 1.15 f_s$. Note the very different spatial structure compared to (*a*) and (*b*).

same as in the unforced state. Given that the phase velocity is equal to the propagation speed of the cores of the vortices, this result confirms that, in lock-in states, a periodic vortex street exists locked-in to the excitation frequency. It also implies that periodic lock-in states in the laminar wake are *non-dispersive*.

Finally, when chaotic states are excited, the wavelength of the vortex street varies significantly along the wake, before a constant value is established far behind the cylinder (figure 23*c*). The substantial variation of the spatial structure along the wake is consistent with the fact that the response states differs from location to location.

5. Discussion

The results obtained in §§3 and 4 suggest the following picture for the development of the response of laminar wakes. In unforced wakes, the vortex-street formation involves two stages. First, a quasi-steady separated flow develops, similar to that obtained for steady-state simulations by Fornberg (1985). Subsequently, unsteady effects appear, as a result of the instability of the separated flow, and lead to the formation of the vortex street. The frequency of the vortex street is however determined by the *absolute instability* of the final time-average flow (Triantafyllou *et al.* 1986), whereas nonlinear effects determine the amplitude of the oscillation. The vortex street is an almost perfectly periodic limit cycle, the frequency of which is a continuous function of the Reynolds number.

In forced wakes, the final, asymptotic state develops from the interaction between two competing patterns, the naturally produced wave, and the forced wave. In the non-lock-in region, the absolute instability of the wake is still the dominant factor in the frequency and state selection process. In this region, the nonlinear interaction between the two patterns plays only a secondary role, which, however, becomes increasingly important as the excitation frequency f_e approaches the boundary frequency f_b. In periodic lock-in states, on the other hand, like the one shown in figure 12(*a*, *b*), a completely reverse picture of the state selection process appears: while the time-average flow is very similar to the flow in the unforced state, indicating that the 'natural frequency' of the flow has not been significantly altered, the frequency and wavelength of the vortex street are very different. This shows that lock-in states result from a purely nonlinear interaction between the two competing patterns, the outcome of which is the complete synchronization of the vortex street with the imposed forcing.

As f_e approaches f_b, an intermediate situation develops, in which the two selection processes (the instability mechanism and the nonlinear interaction) become of comparable importance. The response in this case is characterized by a richness in frequency content and relatively broadband spectral densities. In a very narrow range around the boundary separating the two regions, the two competing patterns create a chaotic response. Consequently, the appropriate scenario describing the development of chaos in laminar wakes is not the RTN scenario, as suggested by Sreenivasan (1985), but the 'pattern competition', proposed by Ciliberto & Gollub (1984) in the context of a different physical problem.

At this point, we would like to note the similarity between our computed spectral densities, and those resulting from the undamped-cylinder experiments of Van Atta & Gharib (1987). Our results suggest that the rich, but not chaotic, spectra measured in their experiments correspond to vibrations of the cylinder in the non-lock-in region; the chaotic spectra occur for vibrations at a frequency very near the boundary frequency f_b. Overall, our results are in total agreement with the conjecture of Van Atta & Gharib (1987) that quasi-periodic and chaotic states appear in laminar wakes only in presence of an external forcing. Our contribution in this respect is in identifying the precise manner through which a simple harmonic forcing can excite quasi-periodic and chaotic states.

The classification of states as a function of the frequency and amplitude of excitation can be simply summarized in a state diagram as follows. For a given amplitude, we can distinguish four important frequencies for the system, which mark the transition between different flow states: the upper and lower boundaries of the lock-in region (f_b^u and f_b^l, respectively), and the upper and lower boundaries of the

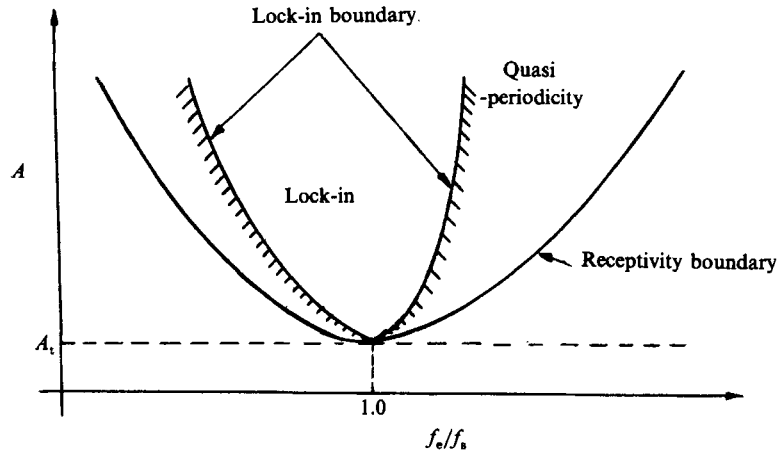

FIGURE 24. State-selection diagram for laminar wakes. The plot should only be interpreted in a qualitative sense. Such regions are referred to in the literature as 'resonant horns' (Arnol'd 1977).

receptivity region (f_r^u and f_r^l). Between the first two frequencies only lock-in states are obtained. Between the lock-in boundary and the corresponding receptivity boundary quasi-periodic non-lock-in states develop. Outside the receptivity region, periodic non-lock-in states, virtually the same as the unforced one, are recovered. Chaotic states develop in a very narrow frequency range around the boundaries of the lock-in region. The extent of the lock-in and receptivity region is amplitude dependent. Both regions are reduced when the amplitude is reduced, and they shrink to zero when the amplitude tends to the threshold amplitude, A_t, required for the excitation to be 'felt' by the wake (see also the discussion at the beginning of §4). For an amplitude of excitation equal to A_t, the wake responds only when the excitation frequency f_e is equal to the Strouhal frequency f_s. Based on these observations, we can sketch the complete form of the state-selection diagram in the frequency–amplitude plane, shown in figure 24. The receptivity and lock-in regions have the form of inverted triangular regions, one inside the other, based on the point $(A = A_t, f_e = f_s)$. This state-selection diagram also represents the stability properties of the naturally produced periodic state. Outside the receptivity region, disturbances are unable to perturb the state of the wake, which can therefore be termed as 'stable'. Inside the receptivity region, however, the periodic state loses its stability, giving rise to quasi-periodic and chaotic states. The inner part of the region is referred to in the literature as 'resonant horn' (Arnol'd 1977). Similar state-selection diagrams have been found in periodically forced chemical systems (Kevrekidis 1987).

The diagram of figure 24 gives only a qualitative summary of the response states of the wake; an exact quantitative diagram is prohibitively expensive, requiring a large amount of computation. Furthermore, we note that the proposed state-selection diagram is valid for finite, but small, amplitudes. For large amplitudes the response may change drastically from the results reported here: for example, additional resonant horns based on subharmonics of the Strouhal frequency may appear; Stansby (1976) has observed that the wake of vibrating cylinders (at high Reynolds numbers) locks-in to frequencies equal to one-half and one-third of the Strouhal frequency. Also, high-amplitude forcing at the Strouhal frequency has been

shown to cause a complete change in the shedding pattern, i.e. shedding of symmetric vortices at twice the Strouhal frequency (Karniadakis *et al.* 1986).

An investigation, currently underway, regarding the state selection in the wake of cylinders oscillating transversely to a steady flow, shows a qualitatively similar behaviour with the one discussed in this section. This further justifies the use of the forcing in the form defined by (9). Preliminary calculations in this case support the results presented here; the regions of state transition are quantitatively different, since the extent and magnitude of excitation are different. In particular, some of the lock-in states described in §4.1 were verified as remaining unchanged in the case of a vibrating single cylinder, as well as in the case of an array of vibrating cylinders placed perpendicular to an oncoming uniform flow. Results for these last two cases will be presented in a future publication.

Before concluding this Section, it is worth discussing whether phenomena of pure fluid-mechanical origin can produce the same result as the forcing used in our calculations. Our results in §3 exclude this possibility for the Reynolds-number regime 0 to 250. At higher Reynolds numbers, however, (e.g. $Re > 2000$) a second pattern may be present, resulting from the instability of the separated shear layer, which introduces a new frequency f_t (Bloor 1964). The interaction of this second pattern with the vortex street has been found by Kutta *et al.* (1987) to cause locally chaotic behaviour in the near wake of the cylinder. The question then is whether this chaotic behaviour can be explained based on the scenario we have presented here. Let us assume that the oscillation of the fluid particles caused by the shear-layer instability can be modelled as an external forcing similar to the one defined in (9). Then, given that the frequency of this second pattern is about five times the Strouhal frequency, the excitation provided by the shear-layer instability lies outside the receptivity range of the wake, and cannot produce chaotic behaviour according to the scenario proposed here. Consequently, the chaotic behaviour reported by Kurta *et al.* (1987) is not produced as a result of 'pattern competition', but is following some diferent route, possibly the RTN scenario.

6. Conclusions

Identification of states in 'open' flow systems is closely related to flow-control problems. One may think, for instance, of the forcing used in the present investigation as loosely representing some 'active control device'. The performance of such a device can be assessed from the final asymptotic state of the flow. Thus, given the state-selection diagram, the following observations can be made.

If cancellation of the vortex street is desired, like in vibration suppression applications, active control devices are ineffective. Owing to the absolute instability of the flow, a large-scale unsteady pattern (vortex street) is always formed. For such applications, therefore, modification of the average flow, such that a convectively unstable wake (no spontaneous unsteady pattern) is obtained, seems a possible alternative.

If reinforcement of the vortex street is desired, like in transport enhancement applications, active control devices can be very effective. Flow destabilization through resonant forcing at the Strouhal frequency is known to cause dramatic improvements in transport rates (Karniadakis *et al.* 1986). The discovery that chaotic states can develop in the wake offers a new possibility for transport enhancement: driving the wake at frequencies capable of creating chaotic states, rather than the Strouhal frequency, in order to exploit the richness of time and

length scales that are present in chaotic states. Investigation of this transport enhancement mode, termed 'chaotic advection' by Aref (1984), is currently underway.

We would like to thank the organizers and participants of the DARPA-URI Conference (July 1987) on *Periodic and Aperiodic Phenomena behind Circular Cylinders* for helpful discussions of a preliminary version of this work. Most of the computations were performed using the CRAY X-MP/48 computer of the Pittsburg Supercomputing Center. One of us (G.S.T.) would like to acknowledge the financial support of ONR under Contract N0014-87-K-0356, and NOAA, under Sea-Grant Contract NA86AA-D-SG089.

REFERENCES

AREF, H. 1984 Stirring by chaotic advection. *J. Fluid Mech.* **143**, 1–21.

ARNOL'D, V. I. 1977 Loss of stability of self-oscillations close to resonance and versal deformations of equivarient vector fields. *Funct. Anal. Appl.* **11**, 85–92.

BERGER, E. & WILLE, R. 1972 Periodic flow phenomena. *Ann. Rev. Fluid Mech.* **4**, 313–340.

BERS, A. 1983 Basic plasma physics I. In *Handbook of Plasma Physics* (ed. M. N. Rosenbluth & R. Z. Sagdeev), vol. 1, chap. 3.2. North Holland.

BLOOR, S. M. 1964 The transition to turbulence in the wake of a circular cylinder. *J. Fluid Mech.* **19**, 290–304.

CHILUKURI, R. 1987 Incompressible laminar flow past a transversely vibrating cylinder. *J. Fluids Trans. ASME Engng* **109**, 166–171.

CHOMAZ, J. M., HUERRE, P. & REDEKOPP L. G. 1988 Bifurcations to local and global modes in spatially developing flows. *Phys. Rev. Lett.* **60**, 25–28.

CILIBERTO, S. & GOLLUB, J. P. 1984 Pattern competition leads to chaos. *Phys. Rev. Lett.* **52**, 922–925.

FORNBERG, B. 1985 Steady viscous flow past a circular cylinder up to Reynolds number 600. *J. Comp. Phys.* **61**, 297–320.

FRIEHE, C. A. 1980 Vortex shedding from cylinders at low Reynolds numbers. *J. Fluid Mech.* **100**, 237–241.

GASTER, M. 1969 Vortex shedding from slender cones at low Reynolds numbers. *J. Fluid Mech.* **38**, 565–576.

GHADDAR, N. K., MAGEN, M., MIKIC, B. B. & PATERA, A. T. 1986 Numerical investigation of incompressible flow in grooved channels. Part 2. Resonance and oscillatory heat transfer. *J. Fluid Mech.* **168**, 541–567.

GRESHO, P. M., CHAN, S. T., LEE, R. L. & UPSON, C. D. 1984 A modified finite element method for solving the time-dependent incompressible Navier–Stokes equations, Part II: Applications. *Intl J. Num. Meth. Fluids* **4**, 619–640.

KARNIADAKIS, G. E. 1988 Numerical simulation of heat transfer from a cylinder in crossflow. *Intl J. Heat Mass Transfer* **31**, 107–118.

KARNIADAKIS, G. E., BULLISTER, E. T. & PATERA, A. T. 1985 A spectral element method for solution of two- and three-dimensional time dependent Navier–Stokes equations. *Proc. Europe–US Conf. on Finite Element Methods for Nonlinear Problems*, pp. 803–817. Springer.

KARNIADAKIS, G. E., MIKIC, B. B. & PATERA, A. T. 1986 Unsteady heat transfer from a cylinder in crossflow; a direct numerical simulation. *Proc. Eighth Intl Heat Transfer Conf., San Francisco*, vol. 2, pp. 429–434. Hemisphere.

KARNIADAKIS, G. E., MIKIC, B. B. & PATERA, A. T. 1988 Minimum dissipation transport enhancement by flow destabilization: Reynolds' analogy revisited. *J. Fluid Mech.* **192**, 365–391.

KEVREKIDIS, I. G. 1987 A numerical study of global bifurcations in chemical systems. *AIChE J.* **33**, 1850.

KOOPMANN, G. H. 1967 The vortex wakes of vibrating cylinders at low Reynolds numbers. *J. Fluid Mech.* **28**, 501–512.

KORCZAK, K. Z. & PATERA, A. T. 1986 An isoparametric spectral element method for solution of the Navier–Stokes equations in complex geometry. *J. Comp. Phys.* **62**, 361–382.

KURTA, A., BOISSON, H. C., CHASSAING, P. & MINH, H. 1987 Nonlinear interaction and the transition to turbulence in the wake of a circular cylinder. *J. Fluid Mech.* **181**, 141–161.

MADAY, Y. & PATERA, A. T. 1987 Spectral element methods for the Navier–Stokes equations. *State-of-the-art Surveys in Computational Mechanics*. ASME.

MCLAUGHLIN, J. & ORSZAG, S. A. 1982 Transition from periodic to chaotic thermal convection. *J. Fluid Mech.* **122**, 123–142.

MORKOVIN, M. V. 1964 Flow around circular cylinders. A kaleidoscope of challenging fluid phenomena. *ASME Symp. on Fully Separated Flows, Philadelphia, Pa*, pp. 102–118.

NEWHOUSE, S., RUELLE, D. & TAKENS, F. 1978 Occurrence of strange axiom A attractors near quasi periodic flows on $T^m, m > 3$. *Commun. Math. Phys.* **64**, 35–40.

PATERA, A. T. 1984 A spectral element method for fluid dynamics: Laminar flow in channel expansion. *J. Comp. Phys.* **54**, 468–488.

RØNQUIST, E. M. & PATERA, A. T. 1987 A Legendre spectral element method for the incompressible Navier–Stokes equations. *Proc. Seventh GAMM Conf. on Numerical Methods in Fluid Mechanics*. Vieweg.

ROSHKO, A. 1954 On the development of turbulent wakes from vortex streets. *Natl Advisory Committee Aeronaut., Rep.* 1191.

RUELLE, D. & TAKENS, F. 1971 On the nature of turbulence. *Commun. Math. Phys.* **20**, 167–192.

SREENIVASAN, K. R. 1985 Transition and turbulence in fluid flows and low-dimensional chaos. In *Frontiers in Fluid Mechanics* (ed. S. H. Davis & J. L. Lumley), pp. 41–67. Springer.

STANSBY, P. K. 1976 The locking-on of vortex shedding due to the cross-stream vibration of circular cylinders in uniform and shear flows. *J. Fluid Mech.* **74**, 641–665.

TRIANTAFYLLOU, G. S., KUPFER, K. & BERS, A. 1987 Absolute instabilities and self-sustained oscillations in the wake of circular cylinders. *Phys. Rev. Lett.* **59**, 1914–1917.

TRIANTAFYLLOU, G. S., TRIANTAFYLLOU, M. S. & CHRYSSOSTOMIDIS, C. 1986 On the formation of vortex streets behind stationary cylinders. *J. Fluid Mech.* **170**, 461–477.

TRITTON, D. J. 1959 Experiments on the flow past a circular cylinder at low Reynolds numbers. *J. Fluid Mech.* **6**, 547.

TRITTON, D. J. 1971 A note on vortex streets behind circular cylinders at low Reynolds number. *J. Fluid Mech.* **45**, 203–208.

VAN ATTA, C. W. & GHARIB, M. 1987 Ordered and chaotic vortex streets behind circular cylinders at low Reynolds numbers. *J. Fluid Mech.* **174**, 113–133.